Calibration of flight model CCDs for CoRoT mission

Vincent Lapeyrere, Pernelle Bernardi, Jean-Tristan Buey, Michel Auvergne, Didier Tiphene

Mon. Not. R. Astron. Soc. **365,** 1171–1179 (2006) doi:10.1111/j.1365-2966.2005.09793.x

Calibration of flight model CCDs for CoRoT mission

V. Lapeyrere,⋆ P. Bernardi, J.-T. Buey, M. Auvergne and D. Tiphène
LESIA, UMR 8109, Observatoire de Paris-Meudon, 5 Pl. Jules Janssen, 92195 Meudon, France

Accepted 2005 October 26. Received 2005 October 24; in original form 2005 August 19

ABSTRACT

CoRoT (Convection, Rotation and Transit) is a mission of high-accuracy photometry with two scientific programmes: asteroseismology and planet finding, using CCDs as detectors. Ten 2048×4096 CCDs manufactured by E2V (42-80) were calibrated on Meudon test bench in order to choose the best ones for flight. A very high instrument stability is needed. Taking into account the environmental perturbations (temperature, attitude control system jitter, radiations, etc.) we studied sensitivity of CCD gain and quantum efficiency to temperature and sensitivity of the output signal to bias voltages. Special attention was paid to pixel capacity and noise sources coming from dark current and pixel response non-uniformity. The calibration results together with the expected voltages and temperature fluctuations are compared with the specifications.

Key words: instrumentation: detectors – space vehicles: instruments – techniques: photometric.

1 INTRODUCTION

The CoRoT (Convection, Rotation and Transit) small satellite is a space mission dedicated to stellar seismology and to the search for extrasolar planets as primary goals. The asteroseismology (AS) channel should be able to detect periodic variations of luminosity comparable to low-degree solar oscillations modes on main-sequence targets brighter than 6 mag and with spectral type between G and A (Baglin et al. 1998). For such stars the amplitudes of solar like oscillations are between 2 and 10 ppm (Samadi & Goupil 2001; Samadi, Goupil & Lebreton 2001) with a typical lifetime of 5 days and periods in the interval 1 min to 3 h. 50–60 stars will be continuously monitored during 150 d.

On the Planet Finder (PF) channel the method is based on the detection of fortuitous transits of planets in front of their parent star. The amplitude of a typical transit is between 7×10^{-5} for telluric planets and 2×10^{-2} for Jupiter-like planets, and its duration is between 3 and 12 h. The largest number of detections will occur for stars with a $m_V = 14$ (Rouan et al. 2000; Borde, Rouan & Leger 2001) and spectral type between K and F. A maximum number of 60 000 stars will be measured during five 150-d runs.

To detect such small variations a high instrumental stability is required (see Auvergne et al. 2003, for a description of the main environmental perturbations). The goal is to keep each white noise contributor at a level smaller than 1/10th of the photon noise for a $m_V = 6$ star and to keep each periodic perturbation due to the orbital motion to a level smaller than 2 ppm.

The focal plane of the CoRoT instrument is composed of four CCDs covering a surface of 2.66 × 3 degrees on the sky. 10 CCDs, 4280 series, were purchased from E2V with CoRoT specifications. All CCDs were characterized with two objectives: select the best four CCDs for flight, and determine parameters which will be used for data corrections.

This paper presents the results obtained during this sorting and calibration process. The testing of a number of CCDs (nine were fully characterized) gives us a good idea of typical characteristic of this kind of CCD.

Section 2 is a short description of CoRoT, the mission and the instrument. Section 3 presents the test bench. In Section 4, we describe all the measurements made on the CCDs. Finally, Section 5 discuses in which way the characteristics measured and CCD defects (traps or high dark current pixels) act on the photometric performance and can be compared to the specifications.

⋆E-mail: vincent.lapeyrere@obspm.fr

2 CoRoT DESCRIPTION

2.1 CoRoT mission

CoRoT is a mission managed by Centre National d'Etude Spatiale (CNES) in association with three major French laboratories and several European countries contributing to the payload and to the ground segment. CoRoT is the third mission on the multimission platform PROTEUS designed for low Earth orbits. The first mission was JASON1, launched in 2001 December. PROTEUS development is carried out under the partnership of the French Space Agency (CNES) and Alcatel Space Industries.

The line of sight of CoRoT is assigned to keep a constant direction during each period of 5 months, with a 90 per cent duty cycle requirement (no occultation by the Earth). As a result, CoRoT has an inertial polar circular orbit, at an altitude of 896 km. The constraints to be taken into account for the orientation of the spacecraft are:

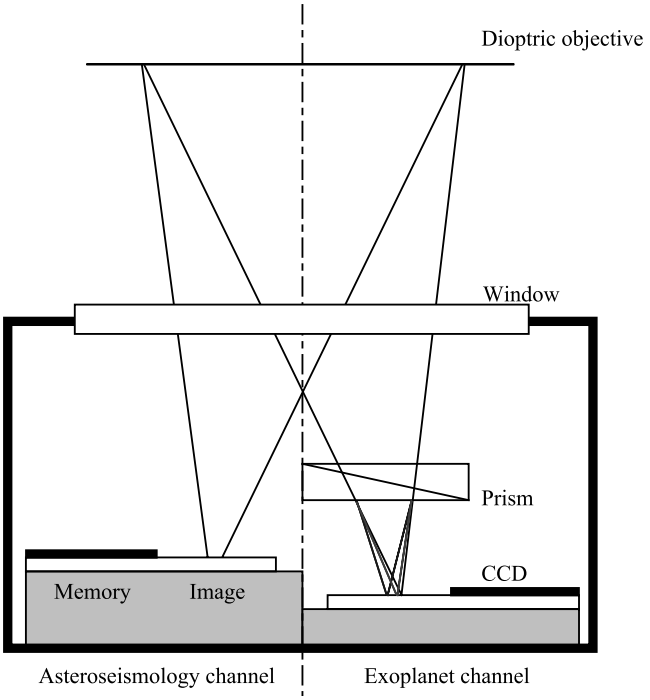

Figure 1. Focal box with two different channels.

(i) Sun glare: the observations are possible when the Sun is at more than 90° of the observed field.

(ii) Stray light from the Earth: the line of sight must remain at more than 16° from the Earth limb. With this constraint and at the altitude of CoRoT, the radius on the sky of the observable zone is 12°.

(iii) Thermal constraints on the focal box radiator which must be in the shadow as much as possible.

Taken together, these constraints lead to one possible mission profile, with two long (150-d) and two short (30-d) runs per year.

2.2 The Payload

The optics has been designed to minimize scattered light at focal plane level. An off-axis afocal telescope and a dioptric objective allow an efficient baffling. CoRoT will collect 7×10^6 e$^-$ per exposure (0.8 s) for a magnitude $m_V = 5.7$ on the AS channel and 1×10^6e$^-$ per exposure (31.8 s) for $m_V = 12$ star on the PF channel. To avoid saturation on such bright target, the images of the AS field are slightly defocused and an image covers approximately 300–400 pixel (Fig. 1). In front of the PF CCDs a prism gives for each target a low-resolution spectrum ($\sim$100 nm pixel^{-1}). For targets with magnitude in the range $11.5 < m_V < 14.5$, three broad-band colours can be measured.

The focal box is cooled by a radiator via a passive thermal link at a temperature around -40°C. The orbital temperature variations of the radiator are filtered by an active control system which maintains the temperature with a stability of $\pm$0.005 K.

The four CCDs are E2V 42-80. They are frame-transfer CCDs with an image area of 2048 × 2048 pixel and a memory area of 2048 × 2054 pixel. They are thinned, back illuminated and used the Advanced Inverted Mode operation (AIMO) to limit the interface dark current. The line-transfer time is 100 μs for AS CCDs and 150 μs on PF channel. The memory zone is read during the following

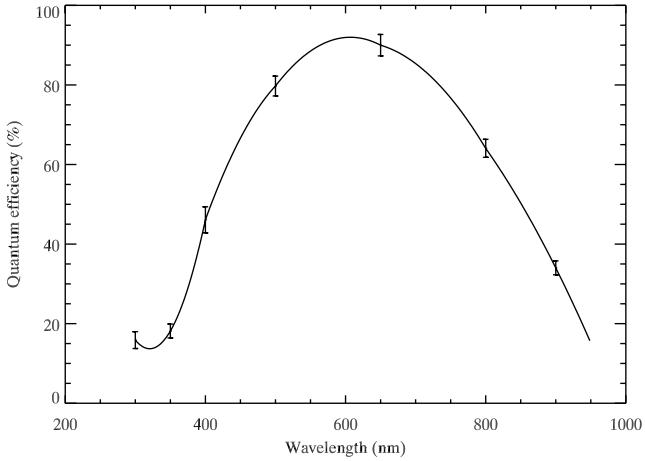

Figure 2. Mean quantum efficiency for the 10 CCDs. Error bars represent the dispersion on all CCDs.

exposure on two outputs. The whole memory zone is read for PF (32-s integration) while ten 50 × 50 pixel windows are read on AS CCDs. Quantum efficiency has been measured by E2V. The mean quantum efficiency on the bandwidth 300–950 nm varies from 60 to 64.5 per cent. The typical quantum efficiency curve is shown in Fig. 2.

The front-end electronics boxes for signal amplification and bias voltages generation are just around the focal box and their temperature stability is better than 0.014 K. The video electronics is on the upper side of the equipment bay which has a passive regulation with two radiators on each side of the satellite (Fig. 3), keeping the temperature at about 16 ± 0.2°C. The expected end-to-end gain sensitivity to temperature is less than 20 ppm K^{-1}.

The attitude control system (ACS) uses the instrument outputs (position error of two AS targets) instead of the information coming from the star tracker in order to elaborate fine angle error data. The star flux is measured by an aperture photometry method. The aperture is adapted to each star and is defined in such a way that the signal-to-noise ratio (which takes into account pointing jitter and crowding as noise sources) of the flux measurement is maximum. When the starlight wanders in and out of the aperture and on pixels with different quantum efficiency, spurious flux variations are produced depending on the aperture size and pixel response nonuniformity.

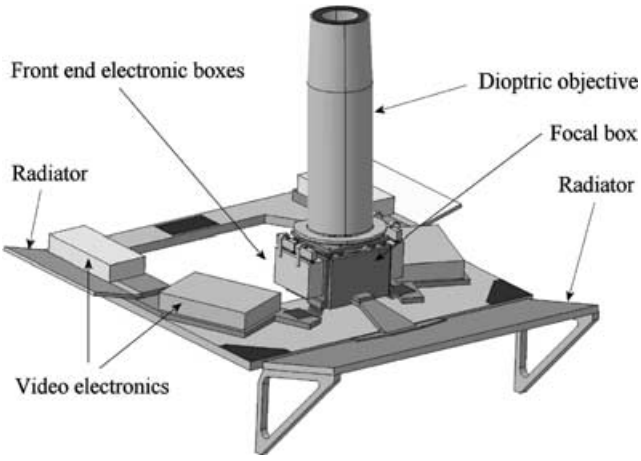

Figure 3. Diagram of the upper side of the equipment bay.

3 THE TEST BENCH

The heart of the experiment consists of the CCD mounted in a cryostat. The CCD is linked to a large metal bar cooled by a cryogenic device (Fig. 4). This bar increases the thermal stability of the CCD. A temperature of −45°C is reached with fluctuations less than 0.01°C.

The CCD is illuminated with light coming from three light-emitting diodes (LEDs) or from a monochromator. LED characteristics are $\lambda = 470$ nm and $\Delta\lambda = 35$ nm for the blue LED; $\lambda = 640$ nm and $\Delta\lambda = 17$ nm for the red LED; $\lambda = 880$ nm and $\Delta\lambda = 80$ nm for the IR LED. In the monochromator, the halogen lamp is stabilized with a current regulation and the bandwidth is adjustable between 10 and 50 nm.

Two light sources are also used to illuminate an integrating sphere in order to obtain a flat illumination of the whole CCD. The intensity of illumination across the field is uniform to within about 5 per cent. In order to mimic star image, a mask consisting of a metal plate drilled with holes can be placed in front of the integrating sphere output. The mask is imaged on to the CCD with an objective. The *F*/4 aperture of this objective reproduces the same photon incidence as that of CoRoT on the CCD.

The standard readout of the CCD is in video mode. The exposure time is therefore controlled by the time between two image transfers in the memory area. The acquisition frequency is 1 image per 32 s. The transfer of the image in the memory area takes 0.2 s, so that the exposure time is 31.8 s. The flux received by the CCD is defined by controlling the LED pulse duration during exposure.

4 CCDS CALIBRATION

4.1 Dark current

The dark current law has the standard form:

$$D(T) = D(T_0)\alpha\, T^3 \mathrm{e}^{-\beta/T}, \quad (1)$$

where $D(T_0)$ is the dark current at 280 K and is equal to 250 $\mathrm{e^-\ pix^{-1}\ s^{-1}}$ for AIMO and to 10^4 $\mathrm{e^-\ pix^{-1}\ s^{-1}}$ for non-AIMO. The α and β values are, respectively, $(1.14 \times 10^6, 122)$ and (9080, 6400). The AIMO is only active when all phases are at 0 V, i.e. when charges are immobile.

The dark current was measured at a temperature of −40°C on series of 30 dark images with 60-s exposures. On these images the mean time spent by charges in the CCD is 71 s – integration plus readout – with 99.2 per cent of this time in AIMO. In this condition and according to equation (1) the expected dark current is about 0.18 $\mathrm{e^-\ pix^{-1}\ s^{-1}}$. The mean values measured are between 0.07 and 0.14 $\mathrm{e^-\ pix^{-1}\ s^{-1}}$ (see Table 1). On the nine CCDs, a total of seven columns with dark current greater than 1 $\mathrm{e^-\ pix^{-1}\ s^{-1}}$ are detected among which four columns are in the range 5–15 $\mathrm{e^-\ pix^{-1}\ s^{-1}}$ (see Table 1).

4.2 Pixel response non-uniformity

The intrapixel non-uniformity (Jorden et al. 1994; Piterman & Ninkov 2002) was not measured because we believe that its impact is small. It has been shown by these studies that when a pixel is illuminated by a spot smaller than the pixel area and moving in the *x* or *y* direction, the flux measured by the illuminated pixel can vary by several tens of per cent but the flux summed over the nine adjacent pixels remains constant to within about 1 per cent and this variation cannot be distinguished from the pixel-to-pixel non-uniformity. This is true only for thinned backside-illuminated CCDs. This 'diffusion' process is negligible for our photometric application, the total flux being measured in a large aperture (300 pixel for AS channel and 80 pixel for PF channel).

Table 1. Dark current measurements at −40°C.

CCD name	Dark current ($\mathrm{e^-\ pix^{-1}\ s^{-1}}$)	No. of columns $> 1\ \mathrm{e^-\ pix^{-1}}\ s^{-1}$
Amon (55)	0.13	2
Apopis (67)	0.08	2
Aton (56)	0.11	3
Benu (76)	0.08	0
Fefket (32)	0.07	0
Iah (71)	0.14	0
Iousaas (33)	0.07	0
Mandulis (45)	0.10	0
Mehen (60)	0.10	0

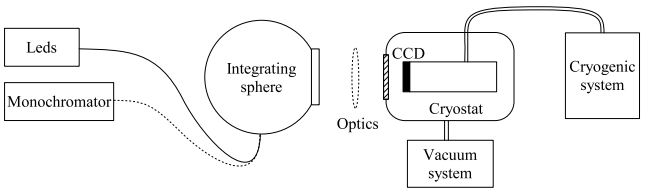

Figure 4. Test bench.

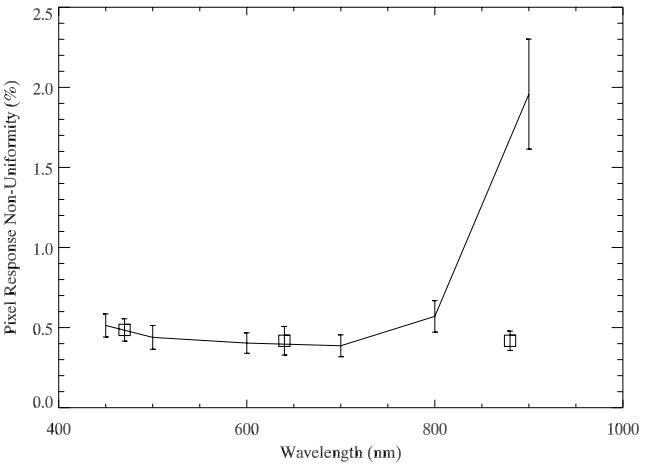

Figure 5. Evolution of local PRNU with wavelength. Measurements made with bandwidth of 10 nm. Error bars represent the dispersion on all CCDs (for wavelength greater than 800 nm, PRNU is dominated by fringing). The three square points represent measurements with LED.

The CCD was illuminated with the integrating sphere. 30 images are summed to reduce readout and photon noise. The measurement accuracy on the relative quantum efficiency is estimated to be less than 0.07 per cent. To reduce the contribution of non-uniform illumination, the local pixel response non-uniformity (PRNU) is computed in windows of 32 × 32 pixel. Fig. 5 shows the evolution of the local PRNU with wavelength measured with a bandwidth of 10 nm.

For all CCDs, the PRNU is lower than 0.6 per cent except for wavelengths greater than 800 nm because of fringing. The evolution with wavelength can be characterized by three different images (see Fig. 6). The flat-field at 450 nm shows structures due to CCD surface, blue photons being absorbed near surface. The flat-field at 650 nm

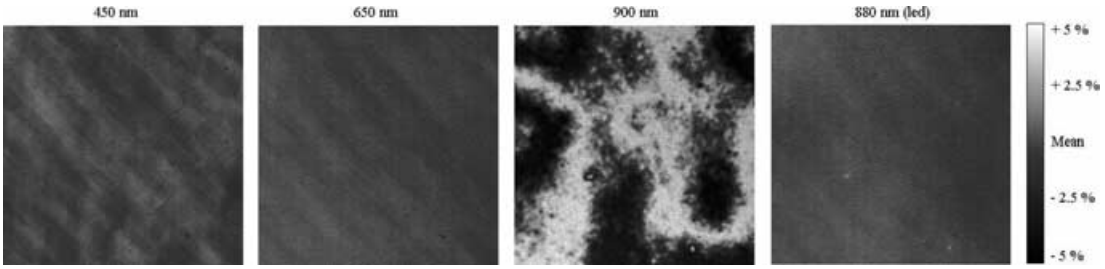

Figure 6. These images represent four portions (300 × 300 pixel) of flat-field images at different wavelengths. The three images on the left-hand panel are obtained with monochromator and bandwidth of 10 nm. The one on the right-hand panel is obtained with IR LED illumination (880 nm and a bandwidth of 80 nm).

shows the best uniformity. Finally, the flat-field at 900 nm shows fringing due to interferences caused by multiple reflections inside the CCD (for IR photon the mean free path is larger than the silicium thickness which is 10 μm). These interferences are only present when the source is monochromatic which is the case on our image (bandwidth of 10 nm). However when the bandwidth is larger, for example, with LED images the fringing entirely disappears as can be seen in the flat-field made with a LED at 880 nm (bandwidth = 80 nm).

We note on flat-field images (on all CCDs) the presence of rows with lower or greater value than the mean value by a few per cent (Fig. 7). These rows are #512, 1024 and 1536, and correspond to junctions between masks of 512 rows used to manufacture CCDs. At these junctions pixels can have a different size which implies a different collecting surface. The quantum efficiency does not differ strongly on these rows, but the difference of collecting surface changes the collecting efficiency.

4.3 Gain of CCD

To measure the CCD gain we measure first the whole gain g and independently the gain of the readout electronics. The CCD gain is then given by the relation:

$$g = \frac{G_{\rm CCD} \times G_{\rm elec}}{G_{\rm adc}}, \tag{2}$$

where $G_{\rm elec}$ is the electronic gain and $G_{\rm adc}$ (μV ADU^{-1}) is the digital conversion factor.

Knowing $G_{\rm elec}$ and $G_{\rm adc}$ it is possible to deduce $G_{\rm CCD}$. According to the gain statistics, it is possible to determine g by the following relation (Janesick 2001):

$$n_{\rm ADU} = g \times \left(\sigma^2_{\rm ADU} - \sigma^2_{\rm r}\right), \tag{3}$$

where $n_{\rm ADU}$ is the mean illumination level, $\sigma^2_{\rm ADU}$ is the variance of the image and $\sigma_{\rm r}$ is the readout noise.

When $n_{\rm ADU}$ is large enough $\sigma_{\rm r}$ is negligible compared to $\sigma_{\rm ADU}$. In this case the slope of the curve variance versus the mean is equal to $1/g$. This is true only if the quantum efficiency is perfectly uniform. To avoid the PRNU contribution to the variance, the variance was computed on the difference of two images with the same mean illumination level. In this case the slope of the relation $n_{\rm ADU} = f(\sigma^2_{\rm ADU})$ is equal to $2g$.

The gain mean value for all CCDs is 4.28 μV E^{-1} with a dispersion of 0.12 μV E^{-1} and the difference between left- and right-hand side outputs is lower than 5 per cent for all CCDs. The precision on the gain measurement is 1 per cent (see results in Table 2).

The gain is measured for different temperatures in order to determine its sensitivity to CCD temperature (Fig. 8). The gain temperature sensitivity $\alpha_{\rm G}$ is defined by

$$\alpha_{\rm G} = \frac{10^6}{G_{\rm CCD}(T_0)} \frac{{\rm d}G_{\rm CCD}}{{\rm d}T}, \tag{4}$$

$\alpha_{\rm G}$ being expressed in ppm K^{-1}.

The mean value for all CCDs is −900 ppm K^{-1} with a dispersion of 100 ppm K^{-1}. The measurement precision is about 15 per cent (see Table 3).

Table 2. CCD gain measurements at −40°C.

CCD name (CCD reference)	Left gain (μV/e$^-$)	Right gain (μV/e$^-$)
Amon (55)	4.38	4.24
Apopis (67)	4.11	4.15
Aton (56)	4.45	4.46
Benu (76)	4.20	4.41
Fefket (32)	4.32	4.37
Iah (71)	4.18	4.08
Iousaas (33)	4.35	4.28
Mandulis (45)	4.31	4.31
Mehen (60)	4.33	4.24

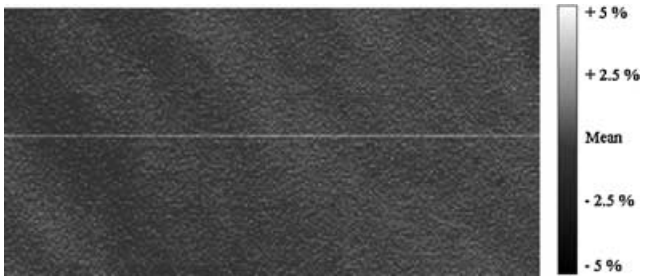

Figure 7. Portion of flat-field showing mask separation.

4.4 Pixel capacity

The pixel capacity depends on the shape of the well which is delimited by phase potential (collecting and barrier phases) and pixel size. During integration, when the Bloomed Full Well (BFW) is passed, the excess of charges spreads symmetrically up and down in the column. During the line transfer, if a charge packet encounters a pixel with a lower BFW than others in the column, the charge excess stays in the upper pixels and produces a charge spreading in the upward direction (see Fig. 9). During transfer, pixel capacity can be

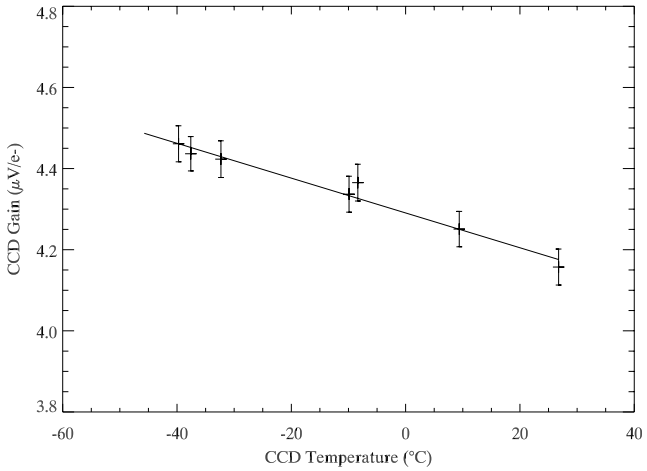

Figure 8. Evolution of CCD gain versus temperature.

Table 3. CCD gain sensitivity to temperature measurements at −40°C.

CCD name	Left sensitivity (ppm K^{-1})	Right sensitivity (ppm K^{-1})
Amon (55)	−872	−927
Apopis (67)	−1136	−999
Aton (56)	−889	−962
Benu (32)	−1398	−453
Fefket (32)	−1036	−1013
Iah (71)	−1024	−626
Iousaas (33)	−817	−910
Mandulis (45)	−919	−781
Mehen (60)	−809	−761

different than during integration because phases are changing and some pixels can need more time to stabilize than others.

In order to characterize the whole surface of the CCD we need a criterion to determine the pixel capacity on flat-field images. Two quantities can be used, the evolution of intensity versus flux or the evolution of variance. The first one shows the break on the linearity curve and the second identifies the case where the Poisson statistic (average equals variance) is no more respected. We use the variance to determine pixel capacity because it is more sensitive.

Flat-field images are taken with white LED illumination and with different flash durations. For each flash time we compute the variance and the average on a difference of two images and on boxes of 40×40 pixel at different positions. For each position we plot the variance and average versus flash duration (see plot in Fig. 10). On this plot the pixel capacity is the average of the image about which the variance is decreasing.

The result on the whole surface of a CCD is presented in Fig. 11. Each square represents the pixel capacity determined in that position. This capacity map shows a difference between the centre and the edges of the CCD. This difference is observed on five of the 10 CCDs tested. The saturation in the centre of the CCD occurs during charge transfer because charges spread in the upward direction. This non-uniformity is explained by the difference between the well shape during transfer at the edges of the CCD (where phases are injected) and the shape in the centre far from the injection point. This difference is due to the resistivity and capacity encountered by phases to reach the centre of the CCD.

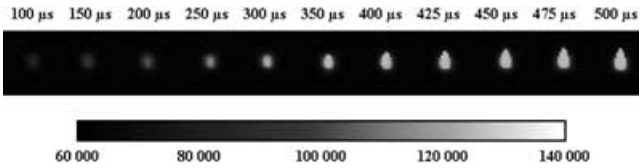

Figure 9. Saturation of a spot image showing spreading in the upward direction for different exposure times. (Pixel capacity is estimated to be 125 ke^{-} pix^{-1}.)

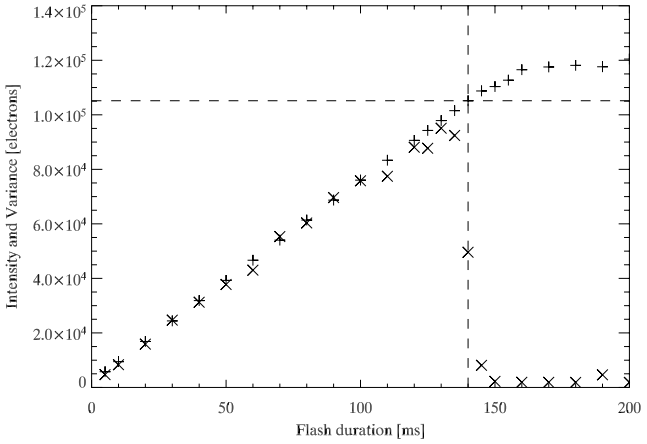

Figure 10. Variance (×) and intensity plus evolution versus flash duration time. The dashed line represents the saturation level.

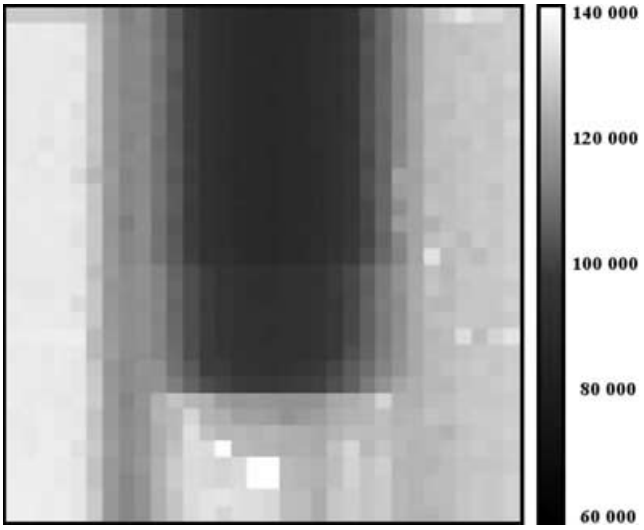

Figure 11. Pixel capacity map (e^{-} $pixel^{-1}$).

In Fig. 11, we can see vertical cut-offs where capacity changes suddenly. These cut-offs occur on rows 512, 1024 and 1536. These rows correspond to junction of masks of 512 rows used to manufacture the CCDs as explained in Section 4.2. These pixels can have a different size. If they are larger, the capacity of this row is bigger and during charge transfer voltages need more time to be stabilized; so BFW can be lower. If they are smaller, the capacity of the well is smaller and the BFW can also be lower. This explains why all pixels above these rows are saturated at a lower level.

For three CCDs we observe a variation greater than 40 per cent on the surface of the CCDs, while for all the others it is lower than

20 per cent except for one with 30 per cent. The BFW is about 150 ke^- $pixel^{-1}$ for all CCDs.

4.5 CCD response sensitivity to temperature

The CCD response is sensitive to temperature due to CCD gain variation as we saw in Section 4.3, but also due to quantum efficiency variation. Quantum efficiency sensitivity (α_{Q_e}) depends on wavelength. The radiometric equation is the following:

$$n_{\rm ADU}(T) = g(T) \int_\lambda n_{\rm p}(\lambda)\, Q_{\rm e}(\lambda, T)\, {\rm d}\lambda, \tag{5}$$

where $n_{\rm ADU}$ is the number of ADU coming from photons (offset and dark current excluded), $n_{\rm p}$ is the number of photons collected by the telescope and arriving on the CCD, $Q_{\rm e}(\lambda, T)$ is the quantum efficiency, $g(T)$ is the gain, T is the temperature of the CCD.

We define the sensitivity to temperature of the CCD gain and quantum efficiency as follows.

$$\alpha_{Q_e}(\lambda, T_0) = \frac{1}{Q_{\rm e}(\lambda, T_0)} \frac{{\rm d}Q_{\rm e}(\lambda, T)}{{\rm d}T}$$

and

$$\alpha_g(T_0) = \frac{1}{g(T_0)} \frac{{\rm d}g(T)}{{\rm d}T} = \alpha_G(T_\theta),$$

with T_0 as reference temperature.

The sensitivity of the CCD response

$$\alpha_{\rm CCD}(T_0) = \frac{1}{n_{\rm ADU}(T_0)} \frac{{\rm d}n_{\rm ADU}(T)}{{\rm d}T} \tag{6}$$

can be written using equation (5) as

$$\alpha_{\rm CCD}(T_0) = \alpha_{\rm G}(T_0) + A_{Q_e}(T_0), \tag{7}$$

where $A_{Q_e}(T_0)$ is the quantum efficiency sensitivity integrated for a source spectrum, defined as

$$A_{Q_e}(T_0) = \frac{\int n_{\rm p}(\lambda)\, Q_{\rm e}(\lambda, T_0)\, \alpha_{Q_e}(\lambda, T_0)\, {\rm d}\lambda}{\int n_{\rm p}(\lambda)\, Q_{\rm e}(\lambda, T_0)\, {\rm d}\lambda}. \tag{8}$$

The CCD response is measured on the test bench for variations of 15° around −40°C, and for three different LEDs. We deduce $\alpha_{\rm CCD}$ which is the slope of this evolution at $T_0 = -45$°C. We find a negative coefficient in the blue LEDs (400–700 nm), and a positive coefficient in the red LEDs (up to 800 nm). Typical values at three different LEDs for all CCDs are given in Table 4. According to equation (7), $A_{Q_e}(T_0)$ can be obtained by subtracting $\alpha_{\rm G}(T_0)$ from $\alpha_{\rm CCD}(T_0)$.

In order to compute the temperature sensitivity for another source spectrum, for example a stellar spectrum, it is necessary to know the evolution of $\alpha_{Q_e}(\lambda, T_0)$ versus λ for a given temperature. It can be ideally measured using a perfect monochromator [$n_{\rm ADU}(\lambda) = \delta(\lambda_0)$]. In that case $\alpha_{Q_e}(\lambda_0, T_0) = A_{Q_e}(T_0)$. On the test bench, we use three LEDs which are not perfectly monochromatic. We can measure an approximation of $\alpha_{Q_e}(\lambda, T_0)$ for three different wavelengths. Results for all CCDs are presented Fig. 12.

Table 4. CCD response sensitivity to temperature [$\alpha_{\rm CCD}(T_0 = -45$°C)].

λ (nm)	470	640	880
Mean value (ppm K^{-1})	−510	−400	2500
Accuracy (ppm K^{-1})	±50	±50	±80
Dispersion (ppm K^{-1})	200	118	360

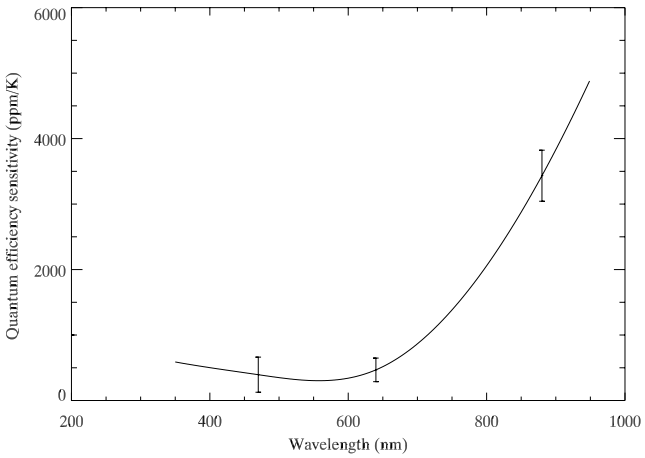

Figure 12. Evolution of the quantum efficiency sensitivity to temperature with wavelength [$\alpha_{Q_e}(\lambda, T_0 = -45$°C)]. Error bars represent dispersion on all CCDs.

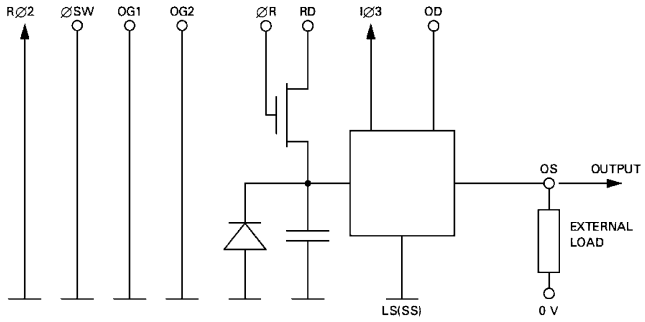

Figure 13. Output circuit of a CCD 42-80 (E2V data sheet).

4.6 CCD sensitivity to bias voltages

A CCD output needs some bias voltages to perform the conversion from electron to voltage. These voltages control the gain of the output amplifier and the collection efficiency of the output amplifier.

For each CCD we verified that the CCD operation is optimum with nominal values of bias voltage. These nominal values come from data sheet and optimization made on engineering model CCDs. When bias voltages vary, some characteristics of the CCDs are modified. In particular, the CCD gain is sensitive to three different parameters which are Vod (output drain), Vog (output gate) and Vrd (reset drain) (see Fig. 13).

Plots in Fig. 14 show the evolution of the video signal amplitude versus each voltage. For each voltage we measure the slope of the curve at the nominal value. These slopes represent the sensitivity to each voltage.

Sensitivity to bias voltages measured on eight CCDs are reported in Table 5.

5 DATA EXPLOITATION

5.1 Application to CoRoT

We will discuss in this section the limitation caused by all these measured parameters on the CoRoT mission.

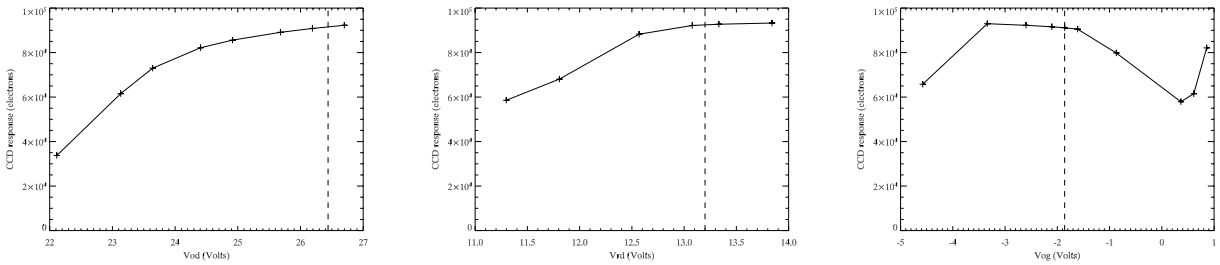

(a) Sensitivity to V_{od} (b) Sensitivity to V_{rd} (c) Sensitivity to V_{og}

Figure 14. CCD response versus voltage amplitude for three different voltages. The dashed line represents the nominal value of the polarization.

Table 5. CCD gain sensitivity to bias voltages.

	Vod	Vrd	Vog
Mean value (ppm mV^{-1})	−34.4	−13.0	22.0
Dispersion (ppm mV^{-1})	3.6	4.0	5.0
Bias voltage value (V)	26.4	13.2	−1.9

5.1.1 Dark current

The problem with the dark current is not its average value which can be measured and subtracted, but the shot noise associated with it. The most sensitive channel to the dark noise is the PF channel because it observes faint stars. The shot noise associated with the mean dark current D (e$^-$ pix^{-1} S^{-1}) integrated over an area $N_{\rm pix}$ (pixels) [area of typical PF channel point spread function (PSF)] during a time T (s) is equal to

$$\sigma_{\rm Dark} = \sqrt{N_{\rm pix} \times T \times D},$$

with the typical values $D = 0.1\,{\rm e}^-\,{\rm pix}^{-1}\,{\rm s}^{-1}$, $N_{\rm pix} = 80$ pixel and $T = 43$ s the dark noise is $\sigma_{\rm Dark} = 18.5\,{\rm e}^-$. This value must be compared with the shot noise of a $m_V = 15$ star observed by CoRoT which is about 200e$^-$. The dark noise is lower than 10 per cent of the photon noise so we can neglect it. Moreover, the mean dark current is negligible in regard to the sky background level which is about $15\,{\rm e}^-\,{\rm pix}^{-1}\,{\rm s}^{-1}$ due to background stars, Earth stray light and zodiacal light.

The dark noise becomes important when white pixels are present. For these bright pixels the dark current can be greater than $10\,{\rm e}^-\,{\rm pix}^{-1}\,{\rm S}^{-1}$. If such a pixel is present in the image of a faint star, the dark current noise can be greater than the specification limit. In that case the star will not be measured.

The influence of irradiation on dark current has been evaluated. The principal conclusion based on analyses of three 42-10 CCDs before and after irradiation concerns dark current. We show that in the case of CoRoT (orbit, shield, etc.) it increases with a rate of 1–$3\,{\rm e}^-\,{\rm pix}^{-1}\,{\rm S}^{-1}\,{\rm Yr}^{-1}$, which represents at the end of the mission a dark current of 3–$10\,{\rm e}^-\,{\rm pix}^{-1}\,{\rm s}^{-1}$. In that case the dark noise becomes $\sigma_{\rm Dark} = \sqrt{80 \times 10 \times 43} = 185\,{\rm e}^-$ in the worst case. This new value is not negligible in regard of the photon noise of a $m_V = 15$ star and of the background level. The consequence is a degradation of the photometric accuracy at the end of the mission.

5.1.2 Pixel response non-uniformity

The PRNU introduces a photometric noise when the image wanders on the CCD. This noise can be evaluated by simulation. We reproduce the typical motion of the theoretical PSF of the instrument on the CCD and we compute the dispersion of the photometric evolution. The mean value is about 5–10 ppm. The dark noise represents less than 1.5 per cent of the photon noise for $m_V = 6$ star in AS channel and less than 0.25 per cent for $m_V = 15$ star in the PF channel. Some regions with black pixels or black columns cause noise greater than 1000 ppm. In this case, the specifications can be exceeded and the star will not be observed on these positions.

5.1.3 CCD sensitivity to temperature

For CoRoT, CCD the temperature oscillation is about 5 mK during the mission. The signal variation due to gain sensitivity associated with this temperature oscillation is about 5 ppm. This amplitude is similar to that of the stellar oscillations to be measured by the AS channel. However, for a more realistic analysis the global response of the CCD must be taken into account (gain plus quantum efficiency sensitivity).

The photometric variation due to CCD response sensitivity to temperature depends on the target spectrum. An evaluation of this variation can be computed for different star spectra with equation (7) and using CoRoT characteristics. For blue targets (with high surface temperature) the sensitivity is negative and for red ones (low surface temperature) it is positive (Fig. 15).

The CCD temperature variation is about 5 mK. Fig. 15 shows that the corresponding variations expected on photometry are lower than 2 ppm, which is marginally within the specification which imposes a threshold of 2 ppm for periodical noise.

5.1.4 Pixel capacity

Pixel capacity is an important parameter for the seismology channel. Principal targets are bright stars ($m_V = 5.7$–6). The photometric

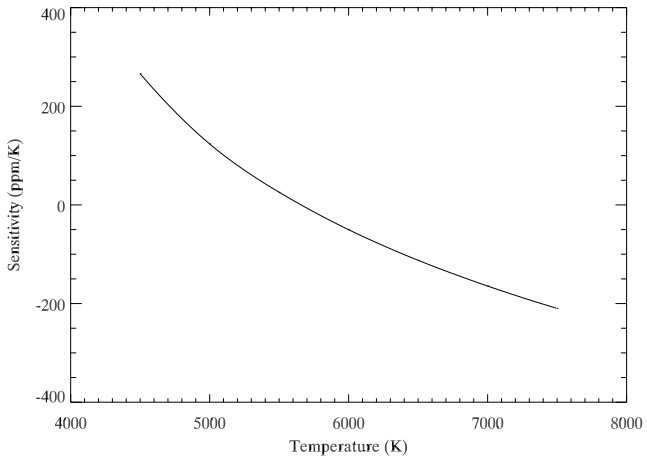

Figure 15. Evolution of sensitivity to CCD temperature versus star surface temperature.

balance implies that a minimum pixel capacity of 80 ke$^-$ pixel^{-1} is needed. Due to uncertainties on the optical model of the instrument, the magnitude of the brightest targets and the value of the CCD quantum efficiency, we keep a margin of 20 ke$^-$ pixel^{-1}. In consequence, we need CCDs with pixels capacity greater than 100 ke$^-$ pixel^{-1} which is not the case on the whole surface of all CCDs.

5.1.5 Sensitivity to bias voltages

Due to the instability of voltages this sensitivity is not negligible and is a greater source of perturbations than temperature sensitivity. These coefficients are measured for all CCDs and will be used for correction of the light curve. These coefficients have to be combined with voltage sensitivities to temperature given by electronics manufacturer (Alcatel), and the temperature variations of electronics. The temperature stability at the orbital frequency of these electronics will be about 1° in the worst case.

The conclusion of this study is that the perturbation due to voltage stability is greater than 33 ppm, while specification for periodical noise is 2 ppm. It is necessary to make corrections on the light curve using coefficients and the different housekeeping data necessary to evaluate voltage evolution.

5.2 Computing the map of defects

There are two different sources of noise related to the CCD surface: the jitter noise which is caused by the movement of the PSF (due to the jitter of the satellite or pointing error) over pixels with different quantum efficiencies and the dark noise which comes from the shot noise of the dark current. It is possible to compute a map of these noises by simulation with dark and flat-field images and to use them to resolve position of defects.

5.2.1 Jitter noise map

We have to compute the jitter noise for each position on the CCD. This can be done knowing the PSF shape (image of a star) and the relative response of each pixel. The PSFs are computed by optical simulation of the instrument and relative response of pixels is measured on the test bench via flat-field images. It is possible to evaluate the flux measured by the CCD for each position by convolution of the flat-field image with the PSF. The jitter noise is the dispersion of fluxes peaked at different positions with a distribution representative of the jitter. In the case of CoRoT the jitter amplitude is 0.2 arcsec, which represents 0.1 pixel. To determine the flux measured for PSF with non-integer coordinates it is necessary to rescale the flat-field image to a size corresponding to the expected accuracy.

To get the right accuracy it is necessary to rescale the flat-field image by a factor of 16. For full-frame CCD images which are 2048 × 2048 pixel the rescaled image is too big to compute a convolution with the PSF in a reasonable time. The calculation can be simplified as follows. We obtain a quantity proportional to the jitter noise when applying a filter on the convolution of the original scale flat-field image with the PSF. The filter used applies to each pixel the dispersion of the 9 pixel contained in 3 × 3 pixel box centred on it. This quantity is a good evaluation of the jitter noise. It is corrected by a factor determined in a small part of the CCD where a more realistic simulation is performed.

As seen in Section 4.2 the PRNU varies with wavelength, and defects are different at 400, 600 or 800 nm. To take into account this evolution it is necessary to compute the jitter noise at different wavelengths. To do that we use three different flat-fields made with the three following LEDs: 470, 640 and 880 nm. These three different flat-fields are convolved with corresponding PSF (i.e. with bandwidth, respectively, 350–550, 550–750 and 750–950 nm). The three convolved images are summed with a weight equal to the mean quantum efficiency of each bandwidth, respectively, 0.65, 0.9 and 0.5. Now, each pixel of the resulting image is equal to the flux integrated in the three different bandwidths. We apply the filter described above and correct the result with a simulation made in the small part of the CCD as explained in the previous paragraph. An example of jitter noise map is presented in Fig. 16.

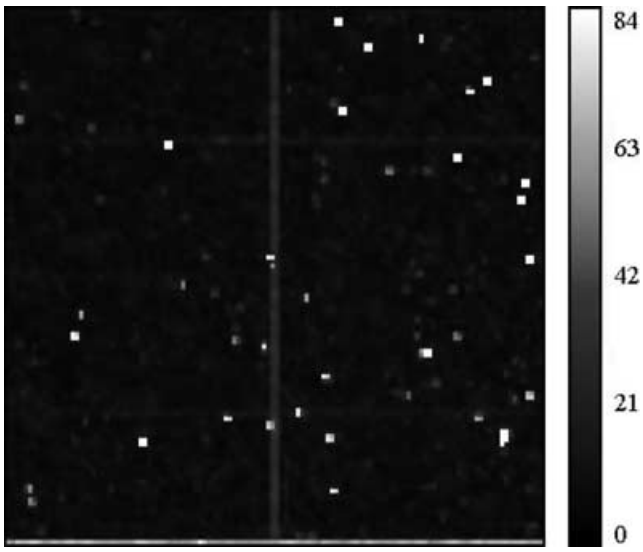

Figure 16. Jitter noise map. Unit is rms noise in ppm.

5.2.2 Dark noise map

For each position of the PSF on the CCD we calculate from the dark image the dark noise which is equal to the square root of the number of electrons contained in the PSF. By this way we obtain a map of the dark current noise.

5.2.3 Defect map

Both noise maps obtained are compared with scientific specifications based on the photon noise; these specifications are different for each channel (PF and AS). The result is a map showing positions where the noise is too high (see Fig. 17). We distinguish two kinds of defects: those due to dark noise (represented in light grey), and those due to jitter noise (represented in dark grey).

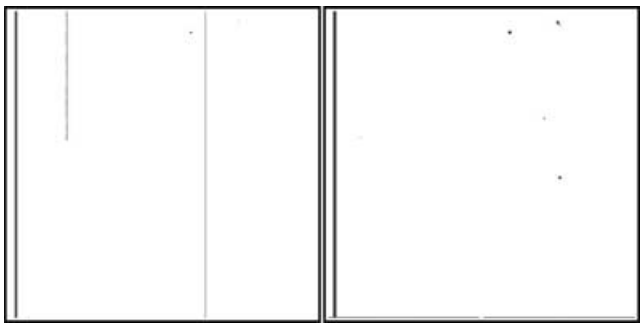

Figure 17. Defect map for exoplanet channel (left-hand panel) and AS channel (right-hand panel).

5.3 Calibration of CCDs

Some perturbations due to the CCD cannot be avoided by selection or stringent specifications on CCDs. Two principal parameters are detected as sources of important perturbations: temperature sensitivity and CCD voltages sensitivity. The objective of calibration is to determine these sensitivity coefficients. This study shows that with expected disturbing amplitudes (temperature and bias voltage), the major perturbation comes from voltage sensitivity.

Coefficients determined during calibration will be used for scientific data corrections. To make these corrections we need information about the evolution of CCD voltages. The telemetry will give us access to several quantities such as electronic temperature and reference voltage value with which it will be possible to estimate evolution of bias voltages.

5.4 Sorting and selection of CCDs

The 10 CCDs have been tested on the test bench. They are all flight models but only four of them will be placed in the focal box. One of the objectives of these tests is to sort the CCDs.

The first step in this section is to determine criteria for this sorting. They must take into account scientific needs, differences between the two channels and different CCD characteristic values.

5.4.1 Sorting criteria

Comparing all these parameters and their consequences we can keep the most important criteria for each channel with a priority order:

Criteria for AS channel:

(i) Pixel capacity is the principal criterion because principal targets are bright star, low pixel capacity CCDs are excluded.

(ii) Jitter noise map is important. However, CoRoT will observe a reduced number of stars on the AS channel (less than 10 per CCD), a few defects are acceptable and constraints can be specified on the instrument pointing to avoid these defects.

Criteria for PF channel:

(i) Dark noise is the principal noise source for faint stars.

(ii) Jitter noise map excludes few positions on large defects.

Points (i) and (ii) are summarized in the defect maps. As the PF channel aims at measuring a large number of stars (up to 6000 per CCD), the surface of defect must be as limited as possible.

(iii) Pixel capacity can increase the saturation problems but only for bright stars which are in minority in PF star sample.

It is possible to sum up this selection into two principal criteria which are: best CCD defects map (including dark defects and PRNU defects) for PF channel in order to observe a maximum number of stars and best capacity for AS channel in order to observe bright stars without saturation problems.

5.4.2 Selection of the CCDs

At the beginning, the 10 CCDs are under the specifications and are able to fly. After the test three CCDs are excluded because good optimizations of bias voltages are impossible and the sensitivities of the gain to the voltages are unusually high. Among the seven CCDs left, three have pixel capacity map with variations greater than 40 per cent on the CCD surface. They are excluded because we do not know their behaviour with the flight model electronic, and this problem could be amplified.

We thus have four CCDs left, and we only need to choose which one will be placed where. The principal criterion for AS is the pixel capacity map. The CCD with the best pixel capacity is allocated to the AS field. Among the three remaining CCDs one has one column of jitter defects placed in the left border of the CCD, and two columns of dark defects are awkward for exoplanet field. Exoplanet field needs CCDs with the best defect map, so this CCD is selected as the second one for AS. The two remaining CCDs are placed on the exoplanet field. Both only have few jitter defects and good pixel capacity.

We also decided for the AS field to place CCDs with the jitter defect column in the position where the column is at the edge of the field.

6 CONCLUSION

CoRoT is a high-accuracy photometer, and the core of this instrument is based on four CCDs (E2V 42-80) AIMO and back illuminated. Some characteristics of these CCDs have an impact on photometric performance: PRNU combined with jitter produces photometric noise, dark current brings shot noise, pixel capacity limits saturation. And others have an impact on photometric stability: gain and quantum efficiency are sensitive to temperature, gain is sensitive to bias voltages.

For the selection of CCD for the CoRoT mission, criteria are based on characteristics affecting photometric performances. The main limitation comes from pixel capacity, and principally the weakness of capacity in the centre of the CCD. On the four selected CCDs the pixel capacity varies from 95 $ke^- pix^{-1}$ in the centre of the worst CCD, to 125 $ke^- pix^{-1}$ at the edges of the best CCD. Presence of defects (dark and PRNU) is very rare on the selected CCDs.

Characteristics affecting stability are considered as calibration parameters. They are used to estimate the perturbation amplitude due to variation of temperature and bias voltages and to make corrections. In the case of CoRoT, the main perturbation comes from sensitivity to bias voltages and particularly to Vod (34 ppm mV^{-1}). With a Vod variation of 1 mV (due to orbital temperature stability of 1 K of the electronic generating the bias), we obtain a perturbation of 34 ppm on the photometric curve. While CCD response temperature sensitivity is lower than 300 ppm K^{-1} and with a orbital CCD temperature variation of 5 mK, the perturbation on photometric curve is lower than 2 ppm.

ACKNOWLEDGMENTS

I am grateful to all the CoRoT team for providing the support for doing this work. I also thank the referee for his helpful remarks.

REFERENCES

Auvergne et al., 2003, Proc. SPIE, 4854, 170A
Baglin A. et al. (the CoRoT Team), 1998, IAUS, 185, 301
Borde P., Rouan D., Leger A., 2001, C. R. Acad. Sci., Paris, t.2, Srie IV, 1049
Janesick, J. R., 2001, Scientific Charge-Couple Devices. SPIE, Bellingham
Jorden P. R., Deltorn J. M., Oates A. P., 1994, Proc. SPIE, 2198, 836
Piterman A., Ninkov Z., 2002, Opt. Eng., 41, 1192
Rouan D., Baglin A., Copet E., Schneider J., Borde P., Deleuil M., Vuillemin A., Leger A., 2000, Earth Moon Planets, 81, 79
Samadi R., Goupil M.-J., 2001, A&A, 370, 136
Samadi R., Goupil M. J., Lebreton Y., 2001, A&A, 370, 147

This paper has been typeset from a TEX/LATEX file prepared by the author.